Available online at www.sciencedirect.com
SCIENCE DIRECT
Journal of Solid State Chemistry 179 (2006) 1356–1362
JOURNAL OF SOLID STATE CHEMISTRY
www.elsevier.com/locate/jssc

Luminescence of $NaGdFPO_4:Ln^{3+}$ after VUV excitation: A comparison with $GdPO_4:Ln^{3+}$ (Ln = Ce, Tb)

Zifeng Tian[a], Hongbin Liang[a,*], Huihong Lin[a], Qiang Su[a,*], Bei Guo[a], Guobin Zhang[b], Yibing Fu[b]

[a]*State Key Laboratory of Optoelectronic Materials and Technologies, School of Chemistry and Chemical Engineering, Sun Yat-sen University, Guangzhou 510275, PR China*

[b]*National Synchrotron Radiation Laboratory, University of Science and Technology of China, Hefei 230026, PR China*

Received 29 November 2005; received in revised form 16 January 2006; accepted 22 January 2006
Available online 23 February 2006

Abstract

The phosphors $NaGdFPO_4:Ln^{3+}$ and $GdPO_4:Ln^{3+}$ (for Ln^{3+} = Ce^{3+} and Tb^{3+}) were prepared by solid-state reaction technique, the VUV–vis spectroscopic properties of the phosphors were investigated, and we vividly compare the luminescence of Ce^{3+} and Tb^{3+} in the hosts. For phosphors $GdPO_4:Ln^{3+}$, the band near 155 nm in VUV excitation spectrum is assumed to be the host-related absorption, and for $NaGdFPO_4:Ln^{3+}$ the absorption is moved to longer wavelength, near 170 nm, showing the P–O bond covalency increased after fluoridation. The *f–d* transitions of Ce^{3+} and Tb^{3+} in the host lattices are assigned and corroborated, and it was found that the 5*d* states are with lower energy in $NaGdFPO_4:Ln^{3+}$ than those in $GdPO_4:Ln^{3+}$. For fluoridation of $GdPO_4:Ln^{3+}$ to $NaGdFPO_4:Ln^{3+}$, the energy change of Ln^{3+} (Ln = Ce, Tb) 5*d* states is consistent with that of host-related absorption.

Keywords: Luminescence; Vacuum ultraviolet; *f–d* transition; Ce^{3+}; Tb^{3+}; $NaGdFPO_4$; $GdPO_4$

1. Introduction

The spectral properties of rare-earth ions activated phosphors in different hosts in vacuum-ultraviolet (VUV) range are gaining more and more attention [1–5]. The research interest is mainly promoted by searching for appropriate phosphors that can be used in plasma display panels (PDPs) and mercury-free lamps. In these devices, the phosphors are excited by VUV photons consisting of the Xe resonance emission line (147 nm) and the Xe_2 molecular emission band (172 nm). The performance and lifetime of a PDP device are strongly related to the nature of phosphors. At present, the PDP phosphors are mainly $(Y,Gd)BO_3:Eu^{3+}$ for red, $Zn_2SiO_4:Mn^{2+}$ for green, and $BaMgAl_{10}O_{17}:Eu^{2+}$ for blue [6]. The first and most common drawback of these phosphors is the lower efficiency (about 1–2 lm/W) in comparison with a cathode ray tube (CRT) (5–6 lm/W) [7]. Hence it is urgent to find proper phosphors for PDPs, and we think that a suitable PDP phosphor will firstly meet some necessary conditions, such as: (1) the host lattice is chemically stable under heating and VUV irradiation, (2) the phosphor shows stronger absorption around 147 and/or 172 nm, (3) the phosphor exhibits intense emission under VUV excitation, good color purity and an appropriate decay time ($<\sim$5 ms). Based on these conditions, we choose $NaGdFPO_4$ as a host lattice in terms of on the following considerations:

(a) Much work [2,3,8–11] has been devoted to improve the efficiency of PDP phosphors, and the most important approach is by quantum cutting (or named as photon cascade emission) processes. These work share some features: firstly, the processes were mainly found in fluorides (and several complex oxides with lower crystal field strength), as these hosts show lower phonon energy; secondly, Gd^{3+} ions (as a sensitizer and an activator) play an important role in the processes; thirdly, though the

*Corresponding authors. Fax: +86 20 84111038.
E-mail address: cesbin@mail.sysu.edu.cn (H. Liang).

0022-4596/$ - see front matter © 2006 Elsevier Inc. All rights reserved.
doi:10.1016/j.jssc.2006.01.044

quantum cutting was fulfilled in fluoride, since fluorides have no absorption around 147 and 172 nm, they are hard to be used in PDPs. (b) Many phosphates exhibit host-related absorption in the range of about 140–180 nm, which are near the emission wavelength of Xe-containing noble gases plasma [7,12–15]. In addition, rare-earth orthophosphates (RPO_4) are known to have good chemical stability under heating and VUV irradiation, and some authors suggested that RPO_4-based phosphors should be used as PDP phosphors [12,13] or co-phosphors [7,14]. For these reasons, we think that a better solution maybe find a $Gd^{3+}/F^-/PO_4^{3-}$-containing host, which is expected to combine the good qualities of fluorides and phosphates. In these phosphors, the host lattices show intensive absorption around 147 or 172 nm and meanwhile the quantum cutting can be realized. The compound $NaGdFPO_4$, because of its $Gd^{3+}/F/PO_4^{3-}$-containing characteristic and chemical stability, is probably a promising host lattice to fulfill these purposes.

The 5*d* states of rare-earth ions play an important role in searching for suitable PDP phosphors, because the 4*f*–5*d* band is with larger optical absorption section relative to the narrow line-like 4*f*–4*f* transition, it can absorb the excitation energy more efficiently. As a systematic investigation, we firstly report the VUV–vis spectroscopic properties of Ce^{3+} and Tb^{3+}-activated $NaGdFPO_4$ in present paper, and by comparing their luminescence with that of $GdPO_4$, we investigated in detail the influence of fluoridation on the energy of the host-related absorption and the 5*d* states of Ce^{3+} and Tb^{3+}.

2. Experimental

The samples were prepared using high-temperature solid-state reaction technique. The reactants are $(NH_4)_2HPO_4$ (A.R.), NaF (A.R.), CeO_2 (99.9%), Gd_2O_3 (99.9%), Tb_4O_7 (99.9%). The appropriate reactants, according to the normal compositions of compounds $Gd_{1-x}Ln_xPO_4$ (Ln = Ce, Tb; x = 0, 0.02, 0.04, 0.06, 0.08, 0.10), were heated at 1100 °C in CO atmosphere. The samples $Gd_{1-x}Ln_xPO_4$ and NaF with mole ratio 1:1.10 were mixed thoroughly and fired at 700 °C for several hours and cooled to room temperature slowly. The final products were obtained by washing the samples with distilled water and then dried. The preparation reactions can be depicted as follows:

(a) $(1-x)Gd_2O_3 + 2(NH_4)_2HPO_4 + 2xCeO_2 + xCO \xrightarrow{1373\,K} 2Gd_{1-x}Ce_xPO_4 + 4NH_3 + 3H_2O + xCO_2$ or,
$2(1-x)Gd_2O_3 + 4(NH_4)_2HPO_4 + xTb_4O_7 + 4xCO \xrightarrow{1373\,K} 4Gd_{1-x}Tb_xPO_4 + 8NH_3 + 6H_2O + 4xCO_2$

(b) $Gd_{1-x}Ln_xPO_4 + NaF \xrightarrow{973\,K} NaGd_{1-x}Ln_xFPO_4$ (For Ln = Ce, Tb)

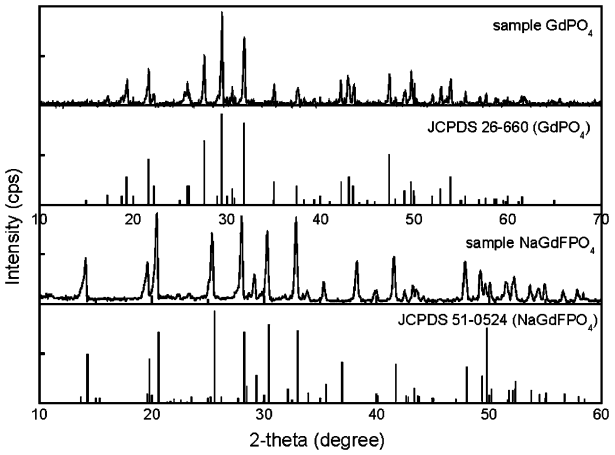

Fig. 1. Powder XRD patterns for the samples $GdPO_4$ and $NaGdFPO_4$.

X-ray diffraction (XRD) measurement of the samples was carried out with Cu$K\alpha$ (λ = 1.5405 Å) radiation. The XRD patterns showed that samples $GdPO_4$:Ln^{3+} were in line with the JCPDS card 26-660, and $NaGdFPO_4$:Ln^{3+} were consistent with the JCPDS card 51-0524, as showed in Fig. 1.

The UV excitation and emission spectra of the phosphors were recorded on a JOBIN YVON FL3-21 spectrofluorometer at room temperature and a 450 W xenon lamp was used as excitation source. The luminescence decay curves were measured at an EDINBURGH FLS 920 combined fluorescence lifetime and steady-state spectrometer, which is equipped with a time-correlated single-photon counting (TCSPC) card. The excitation photons are provided by an nF900 nanosecond flash lamp with pulse width 1 ns and pulse repetition rate 40–100 kHz.

The VUV excitation and corresponding luminescent spectra were measured at the VUV spectroscopy experimental station on beam line U24 of National Synchrotron Radiation Laboratory (NSRL). The electron energy of the storage ring is 800 MeV, and the beam current is about 150–250 mA. A Seya-Namioka monochromator (1200 g/mm, 100–400 nm) is used for the synchrotron radiation excitation photon, while an ARC-257 monochromator (1200 g/mm, 330–700 nm) for the emission photon, and the signal is detected by a Hamamatsu H5920-01 photomultiplier. The resolution of the instruments is about 0.2 nm. The pressure in the sample chamber is about 1×10^{-3} Pa. The relative VUV excitation intensities of the samples are corrected by dividing the measured excitation intensities of the samples with that of sodium salicylate (o-$C_6H_4OHCOONa$) in the same excitation conditions.

3. Results and discussion

3.1. $GdPO_4$ and $NaGdFPO_4$

The VUV excitation spectra for pure $GdPO_4$ and $NaGdFPO_4$ were not depicted before. In addition, the aim of measuring this spectrum is to corroborate the

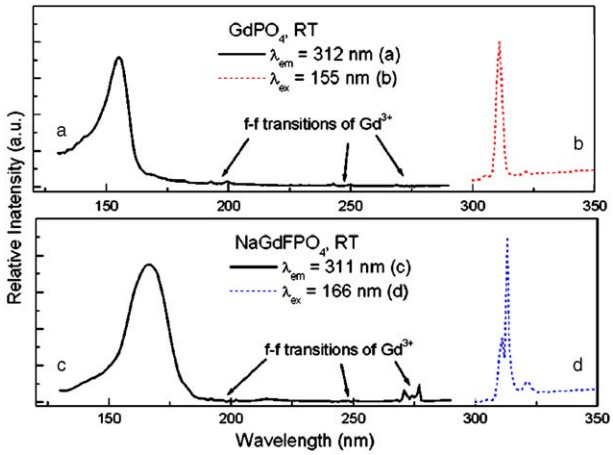

Fig. 2. VUV excitation (a, under emission at 312 nm) and VUV-excited emission (b, excitation under 155 nm) spectra for phosphor $GdPO_4$ at 293 K, the VUV excitation (c, under emission at 311 nm) and VUV-excited emission (d, excitation under 166 nm) spectra for phosphor $NaGdFPO_4$ at 293 K.

position of the host-related absorption. Fig. 2(a) and (c) show the VUV excitation spectra of samples $GdPO_4$ and $NaGdFPO_4$.

For the sample $GdPO_4$, the predominant band with a maximum at 155 nm in VUV excitation curve (solid line a) is assigned to the host-related absorption, which may be the result of intra-molecular absorption of PO_4^{3-} anion in $GdPO_4$. Kunimoto et al. [16] reported the energy transfer between Gd^{3+} and rare-earth ions Pr^{3+}, Nd^{3+}, Tb^{3+} and Tm^{3+} in $GdPO_4$. They found that the fundamental absorption edge of the host crystal was at about 150 nm. Theoretical calculation [17] showed that the lowest intra-molecular $2t_2 \rightarrow 2a$, $3t_2$ transition energy of the tetrahedral PO_4^{3-} molecule was around 7–10 eV. These results coincided with the energy we observed.

The main absorption band is observed peaking at about 166 nm for $NaGdFPO_4$ in Fig. 2(c), which is moved to lower energy region than that in $GdPO_4$. In general, the energy of the host-related absorption is decreased when the bond covalency is increased, as we quasi-quantitatively discussed by the Phillips–van Vechten–Levine dielectric scheme in our previous work [18]. Therefore, the experimental result indicates that the P–O bond covalency is increased for PO_4^{3-} anion in $NaGdFPO_4$ relative to that in $GdPO_4$, and we think that this change might be understood from the following two aspects:

(1) The crystal structural difference between $GdPO_4$ and $NaGdFPO_4$. $GdPO_4$ is crystallized in monoclinic system with space group $P2_1/n$ [19]. Each gadolinium atom is nine-fold coordinated by oxygen atoms in C_s symmetry. The five of nine oxygen atoms form the equatorial pentagonal plane with remaining two oxygen atoms above and other two oxygen atoms below. The coordination of Gd^{3+} in $NaGdFPO_4$ is not available. Only a similar fluorophosphate $NaYFPO_4$ is depicted [20], which is crystallized in the monoclinic system (space group $C_{2/m}$) with the unit cell parameters $a = 8.944(2)$ Å, $b = 6.930(1)$ Å, $c = 6.469(1)$ Å, $\beta = 106.11(3)$ Å, and $Z = 4$. Y^{3+} ions are eight-fold coordinated to form the YO_6F_2 polyhedra. The YO_6F_2 polyhedra form infinite chains along [010] by sharing two *cis*-oxygen atoms, the chains are further linked by the fluorine edges of the YO_6F_2 polyhedra in such a way that, within each chain, the polyhedra alternately have common fluorine atoms with the neighboring chains to their left and right. The two F^- anions occur in a *cis*-arrangement. For the sample $NaGdFPO_4$, we assume that it probably adopts the iso-structure with $NaYFPO_4$ based on the following considerations. First, the similar ionic radii of Gd^{3+} ($R_{Gd(III)} = 1.05$ Å) and Y^{3+} ($R_{Y(III)} = 1.02$ Å) in eight-fold coordination [21]. Second, the similar powder XRD patterns between $NaYFPO_4$ and $NaGdFPO_4$. Third, the similar unit cell parameters [$a = 8.965(5)$ Å, $b = 6.939(1)$ Å, $c = 6.480(3)$ Å, $\beta = 106.18(7)^\circ$, monoclinic, $C_{2/m}$ for $NaGdFPO_4$]. Hence, all four oxygen ions in PO_4^{3-} ions are bound to Gd^{3+} ions in $GdPO_4$, but only three oxygen ions of PO_4^{3-} ions are bound to Gd^{3+} ions in $NaGdFPO_4$, which will elevate the covalency of P–O bond in $NaGdFPO_4$ compared to that in $GdPO_4$. The same effect is observed in silicate apatites like phosphor $La_{9.33}Ce_{0.67}[SiO_4]_6O_2$ [22]. This lattice offers two different sites for La^{3+} ions. One site is seven-coordinated and one of the oxygen ions does not belong to a SiO_4 tetrahedron. The other site is nine-coordinated. On this site, all O^{2-} ions are part of $[SiO_4]$ tetrahedra. The covalency is larger for the seven-fold coordinated site. (2) It is well known that fluorine atoms are with the largest electronegative and exhibit strongest attractive electron ability. After the compound $GdPO_4$ is fluoridated into $NaGdFPO_4$, F^- ions will draw electronic cloud intensive, which will compete with O^{2-} ions, and therefore the ionicity of P–O bond is weakened and the covalency of P–O bond is increased for PO_4^{3-} anion in $NaGdFPO_4$.

Consequently, the intra-molecular absorption of PO_4^{3-} anion is shifted to lower energy in $NaGdFPO_4$ compared to that in $GdPO_4$. In addition, the host-related absorption is thought to be the intrinsic property of this compound. So it has no considerable change when different activators are doped. In order to corroborate the assignment of the host-related absorption for $NaGdFPO_4$ and $GdPO_4$, the optical spectra of $GdPO_4$:Ln^{3+} and $NaGdFPO_4$:Ln^{3+}

Table 1
The host-related absorption band of phosphors $GdPO_4$:Ln^{3+} and $NaGdFPO_4$:Ln^{3+} ($Ln^{3+} = Ce^{3+}$, Tb^{3+})

Phosphor	Figure	Band position (nm)
$GdPO_4$	2	155
$GdPO_4$:Ce^{3+}	3	155
$GdPO_4$:Tb^{3+}	5	156
$NaGdFPO_4$	2	166
$NaGdFPO_4$:Ce^{3+}	3	166
$NaGdFPO_4$:Tb^{3+}	5	170

($Ln^{3+} = Ce^{3+}$, Tb^{3+}) were performed (see following sections) and the host absorption bands were observed and listed in Table 1. It can be found that different doped ions have no considerable influence on the position of host absorption band. The sample $NaGdFPO_4$ exhibits the absorption band near 170 nm, which is very close to the emission wavelength of Xe-containing noble gases plasma. So it is advantageous to absorb the excitation energy in PDP devices or mercury-free lamps.

Upon excitation the host absorption, the emission of Gd^{3+} $^6P_{7/2} \rightarrow {}^8S_{7/2}$ transition at ~311 nm can be observed, as shown in curves (b) and (d). It implies that the host lattice efficiently transfers energy to the Gd^{3+} ions.

3.2. $GdPO_4$:Ce^{3+} and $NaGdFPO_4$:Ce^{3+}

In Fig. 3, the VUV excitation spectrum (curve a) for the sample $Gd_{0.90}Ce_{0.10}PO_4$ is plotted. The broadband peaking at about 155 nm is the host-related absorption, which has been discussed above. To the best of our knowledge, the VUV excitation spectra of YPO_4:Ce^{3+} [4] and $LaPO_4$:Ce^{3+} [23] have been depicted before, but no report was on that of $GdPO_4$:Ce^{3+}. The VUV spectroscopic properties of $GdPO_4$:Ce^{3+} in present work are similar to that of $LaPO_4$:Ce^{3+}, but show some differences from that of YPO_4:Ce^{3+}. For $LaPO_4$:Ce^{3+} [23], the five crystal field splitting components of Ce^{3+} ion were observed with wavelength at 206, 214, 239, 256, and 274 nm, and therefore the barycenter and the crystal field splitting of Ce^{3+} 5*d* states in the host lattice $LaPO_4$ are calculated to be 42.5×10^3 and $12.0 \times 10^3\,cm^{-1}$, respectively. While for YPO_4:Ce^{3+} [4], the five crystal field splitting components were at 323, 248, 237, 227, and 203 nm, the barycenter and the crystal field splitting of Ce^{3+} 5*d* states are

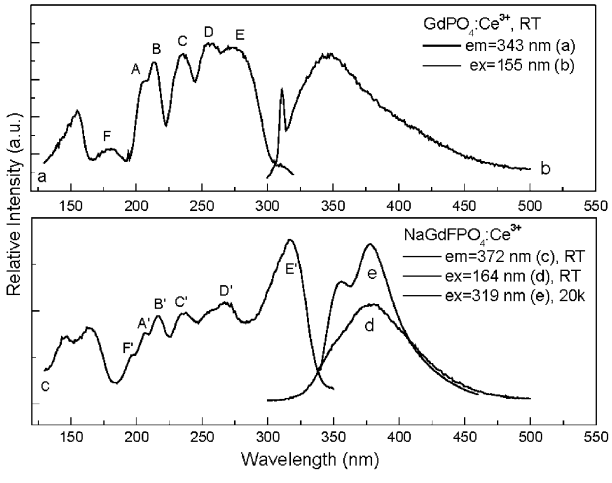

Fig. 3. VUV excitation (a, under emission at 343 nm, RT) and VUV-excited emission (b, excitation under 155 nm, RT) spectra for phosphor $Gd_{0.90}Ce_{0.10}PO_4$. The VUV excitation (c, under emission at 372 nm, RT), VUV-excited emission (d, excitation under 164 nm, RT) and UV-excited emission (e, excitation under 319 nm, 20 K) spectra for phosphor $NaGd_{0.90}Ce_{0.10}FPO_4$.

$41.3 \times 10^3\,cm^{-1}$ and $18.3 \times 10^3\,cm^{-1}$, respectively. In Fig. 3(a), the bands from 200 to 300 nm are connected with the *f*–*d* transition of the Ce^{3+} in $GdPO_4$. The five bands labeled as A (206 nm), B (214 nm), C (236 nm), D (256 nm), and E (274 nm) are thought to be the crystal field splitting (CFS) components for Ce^{3+} 5*d* states in the host lattice $GdPO_4$, respectively. Accordingly, the barycenter and the crystal field splitting are calculated to be 42.6×10^3 and $12.0 \times 10^3\,cm^{-1}$, respectively. The results show that the barycenter is higher and the crystal field splitting is lower for the 5*d* states of Ce^{3+} in $GdPO_4$ and $LaPO_4$ than those in YPO_4.

YPO_4 has the tetragonal zircon structure, the Y^{3+} site is eight-fold coordinated at average bond distance 2.34 Å and with the site symmetry D_{2d} [23,24], while compounds $GdPO_4$ and $LaPO_4$ are of monoclinic monazite structure, the Gd^{3+}/La^{3+} sites are nine-fold coordinated at average bond distance about 2.64/2.50 Å and with the site symmetry C_s [19,24], as mentioned in Section 3.1. The Ce^{3+} 5*d* barycenter positions suggested that the *R*–O (*R* = Y, La, Gd) bond covalency increase according to the relative order $YPO_4 < LaPO_4 \sim GdPO_4$. Correlating this result with the structural characteristics of RPO_4 (*R* = Gd, La, Y), it directly showed that the Ce^{3+} 5*d* barycenter and *R*–O bond covalency mainly related to the nature of the coordination polyhedrons around this ion. The relative lower 5*d* CFS for Ce^{3+} in $GdPO_4$ and $LaPO_4$ is also mainly related to the coordination polyhedrons around Ce^{3+} ion. The different coordination polyhedra determine the CFS of Ce^{3+} 5*d* in YPO_4 and RPO_4 (*R* = La, Gd) firstly. In addition, the bond distance and the coordination number exhibit influence on the magnitude of CFS, and longer bond distance, and higher coordination number will lead to the Ce^{3+} in Gd^{3+}/La^{3+} site experiencing a weaker strength of crystal field effect. Thus the 5*d* crystal field splitting for Ce^{3+} in RPO_4 (*R* = Gd, La) is lower than that in YPO_4.

A weak broad band with a maximum at about 180 nm (labeled as F) was observed in curve a. Because the band does not appear in Fig. 2(a) (the VUV excitation spectrum of $GdPO_4$), we considered that the host absorption or *f*–*d* and charge transfer (CT) transitions of Gd^{3+} were not involved in this band. Apparently, it is related to the absorption of Ce^{3+} or unknown defects and impurities in the host lattice. A similar band was also observed in the VUV excitation spectrum of $LaPO_4$:Ce^{3+} [23]. The weak sharp line peaking at 194 nm is the $^8S_{7/2} \rightarrow {}^6G_{7/2}$ transition of Gd^{3+}. The occurrence of this transition shows the energy transfer between Gd^{3+} and Ce^{3+}.

The VUV-excited emission spectrum for the sample $Gd_{0.90}Ce_{0.10}PO_4$ is shown in Fig. 3(b). Upon 155 nm (the host-related absorption) VUV excitation, both the strong emission around 343 nm of Ce^{3+} and Gd^{3+} ($^6P_{7/2} \rightarrow {}^8S_{7/2}$, 311 nm) can be observed, which implies that the efficient energy transferred between host lattice and Ce^{3+}. The emission of Ce^{3+} is rather broad with the full-width at half-maximum (FWHM) about $6.8 \times 10^3\,cm^{-1}$, and the

characteristic splitting of the emission band Ce^{3+} due to the spin–orbit coupling is not observed, indicating weak spin–orbit coupling of the ground state of Ce^{3+}.

As for $NaGdFPO_4$:Ce^{3+}, the VUV excitation spectrum is shown in Fig. 3(c). The band peaking at 166 nm is assumed to be the host-related absorption as discussed previously.

According to the above-mentioned structural feature of the $NaYFPO_4$ host lattice, we believe that the absorption bands in 200–350 nm are ascribed to be the *f–d* transitions of Ce^{3+} in $NaGdFPO_4$, and the five 5*d* CFS components are marked A′ (206 nm), B′ (216 nm), C′ (236 nm), D′ (267 nm), and E′ (317 nm). At present, we cannot attribute the weak band at about 197 nm (marked as F′), as discussed in the section of $GdPO_4$:Ce^{3+}, which is probably connected with the CT transition for Ce^{3+} or unknown defects and impurities in the host.

The Ce^{3+} 5*d* CFS magnitude in $NaGdFPO_4$ is larger, in contrast to that in $GdPO_4$, which is calculated to be $17.0\times10^3\,cm^{-1}$ in $NaGdFPO_4$ (while it is $12.0\times10^3\,cm^{-1}$ in $GdPO_4$). The barycenter is calculated to be $41.2\times10^3\,cm^{-1}$ for Ce^{3+} 5*d* states in $NaGdFPO_4$, which is lower than that in $GdPO_4$ ($42.6\times10^3\,cm^{-1}$). These results should also be explained by taking into account the coordination polyhedrons around Ce^{3+} and the crystal-field magnitude variation with coordination number for RE sites as discussed above. In addition, the barycenter for Ce^{3+} in $GdPO_4$ and $NaGdFPO_4$ can be quasi-quantitatively compared by the Dorenbos' method as follows.

A semi-empirical model to predict the energy of the 5*d* barycenter energy of Ce^{3+} from the electronegativity χ of the cations is suggested by Dorenbos recently [25].

$$\varepsilon_c = 1.79\times10^{13}\times\sum_{i=1}^{N}\frac{\alpha_{sp}^{i}}{(R_i-0.6\Delta R)^6}, \quad (1)$$

where ε_c is the shift of the barycenter energy in eV relative to the free ion value of 6.35 eV. R_i is the distance (pm) between Ce^{3+} and anion *i* in the undistorted lattice. ΔR is the radii difference between Ce^{3+} and Gd^{3+}, $0.6\Delta R$ is a correction for lattice relaxation around Ce^{3+}. For Ce^{3+} on a Gd^{3+} site, the correction is very small and can be ignored. α_{sp}^{i} ($10^{-30}\,m^{-3}$) is the spectroscopic polarizability of anion *i*, which is closely connected with the polarizability of the anion. The summation is over all *N* anions that coordinate Ce^{3+}. The values of α_{sp} for oxygen and fluorine are against the inverse square of the weighted average of the electronegativity of the cations in the oxide and fluoride compounds, and can be defined as follows:

For oxides (in units of $10^{-30}\,m^3$)

$$\alpha_{sp}^{O} = 0.33+\frac{4.80}{\chi_{av}^2}. \quad (2)$$

For fluorides (also in units of $10^{-30}\,m^3$)

$$\alpha_{sp}^{F} = 0.15+\frac{0.96}{\chi_{av}^2}, \quad (3)$$

where χ_{av} is the weighted average of the electronegativity of the cations.

By this method, the red shift of the barycenter energy is estimated to be about 1.32 and 1.34 eV for Ce^{3+} in $GdPO_4$ and $NaGdFPO_4$, respectively. The results directly show that the decreasing of Ce^{3+} 5*d* barycenter is larger in $NaGdFPO_4$ than that in $GdPO_4$, viz. the 5*d* barycenter is higher in $GdPO_4$ than that in $NaGdFPO_4$.

In Fig. 3(d, e), the emission spectra of $NaGd_{0.90}Ce_{0.10}FPO_4$ at 20 K and RT were recorded upon the host-related absorption at 164 nm and the lowest 5*d* state of Ce^{3+} at 319 nm, respectively. Generally, the Ce^{3+} emission band shows doublet structure due to spin–orbit splitting of the ground state ($^2F_{7/2}$ and $^2F_{5/2}$) with the energy difference $\sim2000\,cm^{-1}$, and the two bands are often resolved much better at lower temperature due to the decrease of the homogeneous line broadening and the electron lattice phonon interaction. This is indeed for $NaGd_{0.90}Ce_{0.10}FPO_4$ at RT and 20 K. A strong broad emission of Ce^{3+} around 372 nm appeared in curve d at RT. When temperature is decreased to 20 K, the doublet band-like emissions with the maxima at about 356 and 378 nm were clearly observed, as shown in Fig. 3(e). According to the emission spectra, the Stokes shift is calculated to be $\sim4.30\times10^3\,cm^{-1}$ for Ce^{3+} in $NaGdFPO_4$. Contrastively, this value is relative larger for Ce^{3+} in $GdPO_4$ ($\sim7.30\times10^3\,cm^{-1}$), indicating smaller electron–phonon coupling for the $5d^1$ state in the host $NaGdFPO_4$ compared to that in $GdPO_4$.

The decay curves of Ce^{3+} emission in $NaGd_{0.90}Ce_{0.10}FPO_4$ at RT are shown in Fig. 4. The curve can be well fitted by single exponential equation

$$I_t = I_0 + A\,\exp(-t/\tau), \quad (4)$$

where *I* and I_0 are the luminescence intensity, *A* is a constant, *t* the time, and τ the decay time for the exponential components. The value of τ is calculated to be about 30.1 ns from the fitted curves.

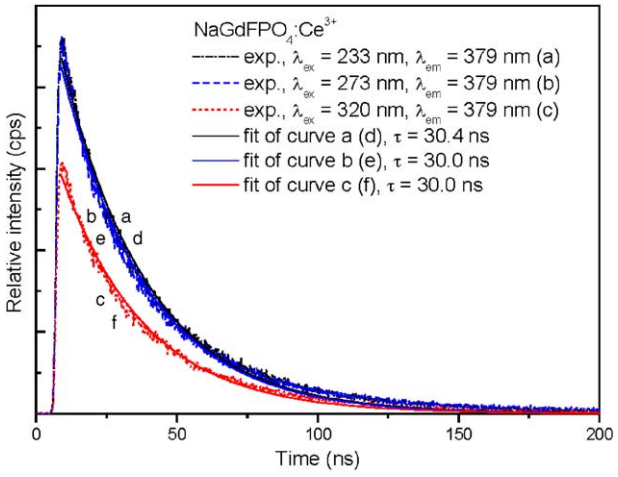

Fig. 4. Decay curves of $NaGd_{0.90}Ce_{0.10}FPO_4$ at RT.

3.3. $GdPO_4:Tb^{3+}$ and $NaGdFPO_4:Tb^{3+}$

The VUV–UV excitation spectra of $Gd_{0.90}Tb_{0.10}PO_4$ and $NaGd_{0.90}Tb_{0.10}FPO_4$ are shown in Fig. 5(a, c). The band peaking at about 156 nm (marked as H) in curve a as well as the band peaking at about 170 nm (marked H′) in curve c are the host-related absorptions, just as that in $GdPO_4:Ce^{3+}$ and $NaGdFPO_4:Ce^{3+}$. The narrow lines peaking at 272 nm is attributed to $^8S_{7/2}\rightarrow{}^6I_J$ transition within Gd^{3+} ions, indicating the existence of the energy transfer from Gd^{3+} to Tb^{3+} in $Gd_{0.90}Tb_{0.10}PO_4$ and $NaGd_{0.90}Tb_{0.10}FPO_4$.

Other broad bands in curves a and c are assignable to the *f–d* transitions of Tb^{3+} in the host lattices, in which the bands A and A′, B and B′ are assigned to the lowest spin-allowed and spin-forbidden *f–d* transitions of Tb^{3+} in $GdPO_4:Tb^{3+}$ and $NaGdFPO_4:Tb^{3+}$, respectively. The assignments can be corroborated as follows. Since the influence of the crystal field and covalency of the host lattice on the red shift of 4*f*–5*d* levels are approximately equal for different rare-earth ions in the same host lattice sites, the lowest 5*d* state energy of different rare-earth ions in same host lattice site can be estimated quantitatively when the lowest 5*d* state energy for one trivalent rare earth in this lattice site is known [25]. The lowest 5*d* states for Ce^{3+} in $GdPO_4:Ce^{3+}$ and $NaGdFPO_4:Ce^{3+}$ are experimentally observed at about 274 and 317 nm, respectively. Consequently, the red shift of the lowest 5*d* states for Ce^{3+} in $GdPO_4:Ce^{3+}$ and $NaGdFPO_4:Ce^{3+}$ are calculated to be about 12.8×10^3 and $17.8\times10^3\,cm^{-1}$ relative to the free Ce^{3+} ion ($49{,}340\,cm^{-1}$) from our experimental results. Considering the red-shift values for Ce^{3+} are accepted for Tb^{3+} in the hosts (also 12.8×10^3 and $17.8\times10^3\,cm^{-1}$ for $GdPO_4:Tb^{3+}$ and $NaGdFPO_4:Tb^{3+}$, respectively), and the lowest 5*d* states for free Tb^{3+} was reported to be about $56{,}200\,cm^{-1}$ (^9D, high-spin) and $62{,}500\,cm^{-1}$ (^7D, low-spin) [26], so the transitions from the ground state ^7F ($4f^8$) to the lowest low-spin (^7D, spin-allowed, strong) and the lowest high-spin (^9D, spin-forbidden, weak) are estimated around 201 and 230 nm for $GdPO_4:Tb^{3+}$, respectively. The bands are labeled as A (204 nm) and B (221 nm) in curve a. Similarly, the lowest spin-allowed *f–d* (^7F–^7D, strong, with higher energy) and the lowest spin-forbidden *f–d* (^7F–^9D, weak, with lower energy) transitions for Tb^{3+} in $NaGdFPO_4:Tb^{3+}$ are estimated around 224 and 260 nm, respectively, which are marked A′ (220 nm) and B′ (260 nm) in curve c. Obviously, the experimental values for both of the lowest spin-allowed *f–d* transitions and the lowest spin-forbidden *f–d* transitions of Tb^{3+} in $GdPO_4:Tb^{3+}$ and $NaGdFPO_4:Tb^{3+}$ are near to their theoretical estimations.

Comparing the curve a with curve c, it is evident that the energy of the 5*d* states for Tb^{3+} in $NaGdFPO_4:Tb^{3+}$ is lower than that in $GdPO_4:Tb^{3+}$, which is in line with the cases for Ce^{3+} in $NaGdFPO_4:Ce^{3+}$ and $GdPO_4:Ce^{3+}$.

One of the purposes for studying the Tb^{3+}-activated phosphors is to find novel green component in PDPs, because the main drawback of current green phosphor $Zn_2SiO_4:Mn^{2+}$ in PDPs is its longer decay time (~12 ms). The phosphors show intensive green emission for series samples $Gd_{1-x}Tb_xPO_4$ and $NaGd_{1-x}Tb_xFPO_4$ ($x=0.02$, 0.04, 0.06, 0.08, 0.10). No significant difference was found in the luminescent curves under UV excitation except for the relative intensities. The samples $Gd_{0.90}Tb_{0.10}PO_4$ and $NaGd_{0.90}Tb_{0.10}FPO_4$ were chosen to measure the VUV spectra, as these phosphors show strongest emission under 273 nm UV excitation. The VUV-excited emission spectra of $Gd_{0.90}Tb_{0.10}PO_4$ and $NaGd_{0.90}Tb_{0.10}FPO_4$ are given in Fig. 5(b, d, e). The characteristic luminescence is due to $^5D_4\rightarrow{}^7F_J$ ($J=4$, 5, 6) transition of Tb^{3+}, the transition $^5D_3\rightarrow{}^7F_J$ is relatively weaker, and the predominant transition is $^5D_4\rightarrow{}^7F_5$ transition peaking at 543 nm, which is advantageous to obtain a phosphor with a good color purity. For these curves, we normalized all parameters those include (emission and excitation) slit width, integrated time, beam intensity and relative intensity of energy at excitation wavelength. Hence, curves b, d, and e directly give the relative emission intensities of samples $GdPO_4:Tb^{3+}$ and $NaGdFPO_4:Tb^{3+}$. It can be found that the phosphor $Gd_{0.90}Tb_{0.10}PO_4$ exhibits stronger emission under 156 nm than that under 172 nm by comparing curves b and d, which is apparent because of the relatively stronger absorption at 156 nm than that at 172 nm as showed in curve a. In order to evaluate the possibility of using $GdPO_4:Tb^{3+}$ or $NaGdFPO_4:Tb^{3+}$ as potential green phosphors in PDPs, normalized spectroscopic curves of commercial PDP green phosphor $Zn_2SiO_4:Mn^{2+}$ are measured as a reference at same conditions and results are shown in curves f–h. It can be observed that the relative luminescent intensity of $NaGd_{0.90}Tb_{0.10}FPO_4$ is higher than that of $Gd_{0.90}Tb_{0.10}PO_4$ and is lower (<60%) than that of commercial PDP green phosphor $Zn_2SiO_4:Mn^{2+}$ under 172 nm excitation.

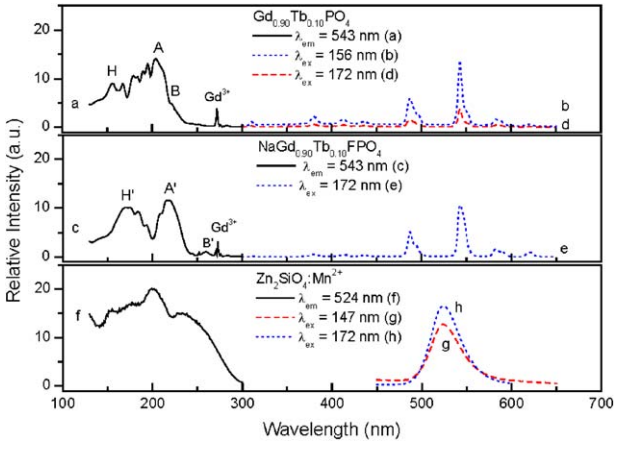

Fig. 5. VUV excitation spectra of $Gd_{0.90}Tb_{0.10}PO_4$ (a, under emission at 543 nm, RT), $NaGd_{0.90}Tb_{0.10}FPO_4$ (c, under emission at 543 nm, RT), and commercial $Zn_2SiO_4:Mn^{2+}$ (f, under emission at 524 nm, RT). The VUV-excited emission spectra of $Gd_{0.90}Tb_{0.10}PO_4$ (b and d, excitation under 156 and 172 nm, RT), $NaGd_{0.90}Tb_{0.10}FPO_4$ (e, excitation under 172 nm, RT), and commercial $Zn_2SiO_4:Mn^{2+}$ (g and h, excitation under 147 and 172 nm, RT).

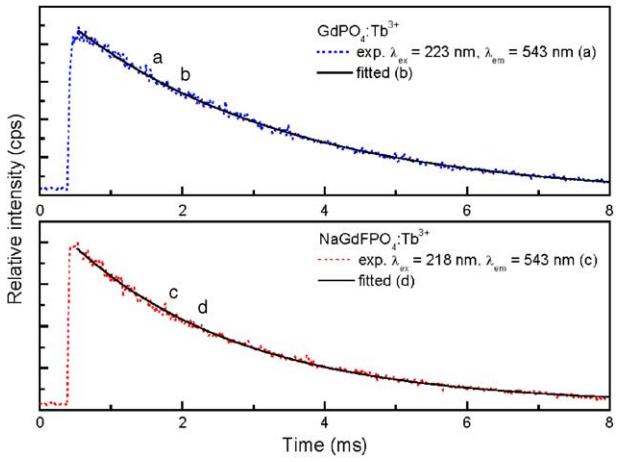

Fig. 6. Decay curves for 543 nm Tb^{3+} emission under 223 nm (a), excitation in $Gd_{0.90}Tb_{0.10}PO_4$ and excitation at 218 nm (c), in $NaGd_{0.90}Tb_{0.10}FPO_4$.

The luminescence decay time (τ) of Tb^{3+} ions was measured to be $\tau = 2.42 \pm 0.02$ ms in $Gd_{0.90}Tb_{0.10}PO_4$ ($\lambda_{ex} = 223$ nm, $\lambda_{em} = 543$ nm) and $\tau = 3.10 \pm 0.03$ ms in $NaGd_{0.90}Tb_{0.10}FPO_4$ ($\lambda_{ex} = 218$ nm, $\lambda_{em} = 543$ nm), which were shown in Fig. 6. The decay time of a PDP phosphor is generally required to be less than 5 ms. It can be found that both $NaGd_{0.90}Tb_{0.10}FPO_4$ and $Gd_{0.90}Tb_{0.10}PO_4$ meet this requirement. Since phosphor $NaGdFPO_4:Tb^{3+}$ shows strong and broad absorption around 170 nm, intensive $^5D_4 \rightarrow {}^7F_5$ emission and an appropriate decay time, it is expected to be a candidate used as green-emitting component in PDPs.

4. Conclusions

The phosphors, $Gd_{1-x}Ln_xPO_4$ and $NaGd_{1-x}Ln_xFPO_4$ (Ln = Ce, Tb; $x = 0$, 0.02, 0.04, 0.06, 0.08, 0.10), were prepared by high temperature solid-state reaction technique, and the VUV–vis luminescent properties were investigated. The differences on the energies of the host-related absorption and the rare-earth 5*d* states in the two hosts were compared and discussed. The PO_4^{3-} absorption bands were observed with maximums near 155 nm in $GdPO_4$ and about 170 nm in $NaGdFPO_4$, which is moved to lower energy region due to the depression of P–O bond intensity after fluoridation. Comparing the barycenter of Ce^{3+} 5*d* states in the host $NaGdFPO_4$ with that in the host $GdPO_4$, it was found that the barycenter of Ce^{3+} 5*d* states is decreased after fluoridation. This change is thought to be the result of increasing the covalency of *Ln*–O bond and spectroscopic polarizability of anion O^{2-} after fluoridation. Similar change is observed in Tb^{3+}-doped samples. Because of the alteration for the coordination polyhedra after fluoridation, the Ce^{3+} 5*d* crystal field splitting is enhanced. $NaGdFPO_4:Tb^{3+}$ has stronger absorption around 172 nm, higher $^5D_4 \rightarrow {}^7F_5$ emission intensity under 172 nm VUV excitation, and a shorter decay time, which is probably a candidate of green PDP phosphor.

Acknowledgments

The work is financial supported by the National Natural Science Foundation of China (20571088), the Science and Technology Project of Guangdong province (2005A10609001, 2005B10301016) and the NSRL innovation foundation of Ministry of Education of China (20041226S).

References

[1] T. Jüstel, H. Nikol, C. Ronda, Angew. Chem. Int. Ed. 37 (1998) 3084.
[2] R.T. Wegh, H. Donker, K.D. Oskam, A. Meijerink, J. Lumin. 90 (2000) 111.
[3] L. van Pieterson, M.F. Reid, R.T. Wegh, S. Soverna, A. Meijerink, Phys. Rev. B. 65 (2002) 045113.
[4] R.T. Wegh, H. Donker, K.D. Oskam, A. Meijerink, J. Lumin. 82 (1999) 93.
[5] R.T. Wegh, E.V.D. van Loef, A. Meijerink, Phys. Rev. B. 65 (2002) 045114.
[6] T. Jüstel, J.-C. Krupa, D.U. Wiechert, J. Lumin. 93 (2001) 179.
[7] R.P. Rao, J. Electrochem. Soc. 150 (8) (2003) H165.
[8] J.L. Sommerdijk, A. Bril, A.W. de Jager, J. Lumin. 9 (1974) 288.
[9] A.M. Srivastava, D.A. Doughty, W.W. Beers, J. Electrochem. Soc. 143 (12) (1996) 4113.
[10] A.M. Srivastava, W.W. Beers, J. Lumin. 71 (1997) 285.
[11] A.M. Srivastava, D.A. Doughty, W.W. Beers, J. Electrochem. Soc. 144 (1997) L190.
[12] W.H. Di, X.J. Wang, B.J. Chen, H.S. Lai, X.X. Zhao, Opt. Mater. 27 (2005) 1386.
[13] W.H. Di, X.J. Wang, B.J. Chen, X.X. Zhao, Chem. Lett. 34 (2005) 566.
[14] R.P. Rao, J. Lumin. 113 (2005) 271.
[15] H.B. Liang, Y. Tao, J.H. Xu, H. He, H. Wu, W.X. Chen, S.B. Wang, Q. Su, J. Solid State Chem. 177 (2004) 901.
[16] Y. Sato, T. Kumagai, S. Okamoto, H. Yamamoto, T. Kunimoto, Jpn. J. Appl. Phys. 43 (6A) (2004) 3456.
[17] S. Saito, K. Wada, R. Onaka, J. Phys. Soc. Jpn. 37 (1974) 711.
[18] H.B. Liang, J.S. Shi, Q. Su, S.Y. Zhang, Y. Tao, Mater. Chem. Phys. 92 (1) (2005) 180.
[19] D.F. Mullica, D.A. Grossie, Inorg. Chim. Acta. 109 (1985) 105.
[20] M.G. Zhizhin, A.V. Olenev, F.M. Spiridonov, L.N. Komissarova, O.G. D'yachenko, J. Solid State Chem. 157 (2001) 8.
[21] R.D. Shannon, Acta Crystallogr. A 32 (1976) 751.
[22] M.J.J. Lammers, G. Blasse, J. Electrochem. Soc. 134 (1987) 2068.
[23] E. Nakazawa, F. Shiga, Jpn. J. Appl. Phys. 42 (2003) 1642.
[24] P. Dorenbos, Phys. Rev. B. 64 (2001) 125117.
[25] P. Dorenbos, J. Lumin. 105 (2003) 117.
[26] P. Dorenbos, J. Lumin. 91 (2000) 91.